Bernardo A. da Silva, Vinicius de Souza Godim de Oliveira, Marco Di Luccio, Dachamir Hotza, Kurosch Rezwan, Michaela Wilhelm

Characterization of functionalized zirconia membranes manufactured by aqueous tape casting

Recommended Citation (primary publication/Version of Record) incl. DOI:

Bernardo A. da Silva, Vinicius de Souza Godim de Oliveira, Marco Di Luccio, Dachamir Hotza, Kurosch Rezwan,
Michaela Wilhelm,
Characterization of functionalized zirconia membranes manufactured by aqueous tape casting,
Ceramics International,
Volume 46, Issue 10, Part B, 2020, Pages 16096-16103, ISSN 0272-8842,
https://doi.org/10.1016/j.ceramint.2020.03.162.

Take down policy
If you believe that this document or any material on this site infringes copyright, please contact publizieren@suub.uni-bremen.de with full details and we will remove access to the material.

Characterization of functionalized zirconia membranes manufactured by aqueous tape casting

Bernardo A. da Silva[a,b], Vinicius de Souza Godim de Oliveira[a,b], Marco Di Luccio[a], Dachamir Hotza[a], Kurosch Rezwan[b,c], Michaela Wilhelm[b,*]

[a] Department of Chemical and Food Engineering (EQA), Federal University of Santa Catarina (UFSC), Florianópolis, SC, 88040-900, Brazil
[b] University of Bremen, Advanced Ceramics, Am Biologischen Garten 2, IW3, D-28359, Bremen, Germany
[c] MAPEX Center for Materials and Processes, University of Bremen, 28359, Bremen, Germany

ABSTRACT

In this study, porous zirconia membranes were developed by aqueous tape casting. The influence of poly (methyl methacrylate) (PMMA) as a pore former, and sintering temperatures (1300, 1400, and 1500 °C) on open porosity and pore size was investigated. The rheological behaviour of the suspensions was measured. The slurries showed pseudoplastic behavior, which is desirable for tape casting. Functionalization with an amino silane precursor (3-aminopropyl triethoxysilane, APTES) was carried out to increase the hydrophilic properties of the membranes. The functionalized samples were characterized by SEM-EDX to identify the moieties attached to the surface. Membranes with open porosity ranging from 27% to 51% and average pore sizes from 0.2 to 1.4 μm were obtained. Samples sintered at 1400 °C with added pore former yielded the highest water flux, 257 $Lm^{-2}h^{-1}$, which increased to 642 $Lm^{-2}h^{-1}$ after functionalization. Membranes with tailored porosity and pore size obtained in this study are indicated for applications involving separation processes, especially for microfiltration systems.

1. Introduction

Tape casting is a well-established process used in large-scale manufacturing of ceramic substrates and layered structures for capacitive electronic application and filtration processes [1]. The process begins with the preparation of a suspension of the ceramic powder in a solvent, with the addition of binder, plasticizer and dispersant [2]. The dispersant controls the stability and rheological behavior of the slurry while the binder and plasticizer confer strength and flexibility to the green tapes. The suspensions are cast onto a stationary or moving surface by flow under a rigid body, called doctor blade, which controls the thickness of the cast film. Then, the tape is dried until the solvent is evaporated. Finally, the tape is cut to the appropriate shape, eventually pressed into a laminate, and sintered [1,2].

Depending on the composition of the ceramic powder, a variety of non-aqueous organic solvents can be used such as ketones, alcohols, and hydrocarbons [1]. Nevertheless, water-based tape casting has been gaining some space in the research and industry [3]. Water as a solvent has the advantage of being non-toxic, non-flammable, easily available and low-cost [3]. Aqueous tape casting is a process able to produce flat ceramic components with tailored thickness and it has been also applied in the manufacturing of porous ceramics materials, which combines the aforementioned advantages of water as solvents with the ability to produce ceramic components with interesting properties. On the other hand, porous ceramics can also be produced by non-aqueous tape casting which leads to similar surface characteristic as similar water flux suggest. ZrO_2 membranes produced with aqueous and non-aqueous tape casting show a wide range of pores between 0.2 nm up to 0.2 μm with water flux values ranging from 400 $Lm^{-2}h^{-1}·bar^{-1}$) up to 1500 $Lm^{-2}h^{-1}·bar^{-1}$) [4].

There are some alternative techniques that can be used to produce porous ceramics membranes [5]. Sacrificial pore formers may be incorporated into the slurries to act as place holders, which will be removed during sintering, such as organic substances (cellulose, starch, etc), or inorganic compounds (graphite, nickel, etc). The technique of sacrificial pore former has been widely used due to the easiness of controlling porosity, pore morphology and pore size distribution in the final ceramic. The tailored parameters are based on the proper selection of the sacrificial pore former. Ceramic membranes have higher chemical, mechanical and thermal stability compared to polymeric membranes and thus show more potential applications. Due to their improved resistance, they can withstand backflushing procedures to

---

remove the fouling layer and improve flux, without damage to their selective surface layer. The low toughness of ceramic membranes appears as a major limitation, which is why zirconium oxide is preferred to other ceramic materials [6].

Zirconia ceramics are known for their toughness and chemical stability. A ceramic membrane has a longer lifetime and higher fluxes at low pressures. Wang et al. [7] suggested the use of 8 mol% YSZ as a solution as membrane materials since increased high-temperature stability helps to avoid cracks in the membrane matrix during sintering.

Functionalization approaches can be performed to increase the hydrophilicity, which can increase the water flux due to the hydrogen bonding onto the ceramic surface. Silanization can be carried out on any type of material and has been widely used to promote new functionalities of the surface of the materials [7]. The functionalization step although not intensively studied in this work confirms the fact that surface modification can increase the water flux in ceramic membranes.

The manufacturing of zirconia membranes for application in microfiltration was already described in the literature [4]. However, to the best of our knowledge, the functionalization of ZrO_2 surfaces to improve water flux in microfiltration systems was not yet investigated. Therefore, the functionalization of the material was carried out by silanization to increase hydrophilicity [7].

In this work, poly (methyl methacrylate) (PMMA) is used as a pore former in an aqueous tape casting process for producing yttria-stabilized zirconia (YSZ) membranes. The aim is to produce amino-silanized YSZ membranes with controlled porosity combined with a high permeate flux aiming at the application in microfiltration processes.

2. Experimental

2.1. Materials

Zirconia powder stabilized with 8% yttria (8YSZ, cubic zirconia, Innovnano, 99.9% purity), with average particle size 450 nm and specific surface 28.53 m^2g^{-1}, was used as ceramic powder; a solution of ammonium polyacrylate (Darvan 821 A, Vanderbilt), as dispersant; and a styrene-acrylic latex emulsion, as binder (Mowilith LDM 6138, Clariant). Poly(methyl methacrylate) (PMMA) was added as a pore-forming agent and produced following the procedure described elsewhere [8], with an average particle size of 3.4 μm, $M_w = 1.4 \times 10^6$ g/mol and a specific surface area of 1.85 $m^2 \cdot g^{-1}$. Finally, cocamide DEA as a surfactant and an aqueous-silicone emulsion (Y-30 Emulsion, Sigma Aldrich) as an anti-foaming agent (or defoamer) were also added to the mixture.

2.2. Slurry preparation and tape casting

Aqueous slurries were prepared by de-agglomeration of 8YSZ and PMMA powders in deionized water with 1 wt% dispersant by ball milling for 24 h. Binder, defoamer and surfactant were added, and the slurry was ball milled for 30 min. The slurry was then left to rest for 2 h to remove air bubbles. The composition of the slurries (Table 1) was

Table 1
Slurry compositions.

Component	Function	YSZ_NPF (wt.%)[a]	YSZ_PF (wt.%)[a]
8YSZ	Ceramic powder	30	24
PMMA	Pore former	–	6
H_2O	Solvent	52	52
Darvan 821	Dispersant	1	1
Mowilith LDM 6138	Binder	15	15
Cocamide DEA	Surfactant	1.5	1.5
Y-30	Anti-foamer	0.5	0.5

[a] YSZ_NPF and YSZ_PF = yttria-stabilized zirconia without pore former and with pore former, respectively.

optimized from a range of solid loadings (20 to 55 wt. %) according to the supplier datasheets, previous experience of the group and processability parameters [9].

The slurries were cast with a tape caster (CC-1200, Mistler) onto a moving support film of polyethylene terephthalate (PET, Mylar®) with a fine coating of silicone layer (G10JRM, Mistler). The casting speed was set at 1 mm/s and the gap between the blade and the carrier was adjusted manually. In order to obtain a final tape thickness of 0.2 to 0.3 mm after drying, a second layer above the green body was carried out, in a process generally referred to as sequential casting [10,11].

2.3. Slurry characterization

The rheological behavior of the slurry was measured in a rotational rheometer (Kinexus Pro+, Essentials, Malvern) at room temperature. The rheogram of the slurry was made at a shear rate of 0.01 to 500 s^{-1} at pH = 9.

Zeta potential of the dispersion of YSZ in deionized water was measured at various pH levels. YSZ (1 wt%) was dispersed in water using 1 wt% dispersant (Darvan 821 A, R. T. Vanderbilt) related to the powder and sonicated for 10 min at 10 W. The measurements were carried out in a zeta potential and particle size meter based on acoustic and electroacoustic spectrometer (DT 1200, Dispersion Technology). For titration, aqueous solutions of KOH and HCl (1 mol L^{-1}) were used.

2.4. Thermal treatments and functionalization

The drying parameters of the tapes were defined by an experimental design combining three different temperatures (20, 35 and 50 °C), and relative humidity values (55%, 70%, and 85%), respectively, using a climate chamber (Model BD 56, Binder) for 24 h. The temperature (20 °C) and relative humidity (85%) at which no cracks or warping in the green tapes were detected were then used in all further assays.

For debinding and sintering, the tapes were cut into 2 × 2 cm samples and placed on an alumina plate and covered with alumina slides to prevent warping. The elimination of the solvent and the burning off of polymer additives were obtained by slow heating (1 °C/min) up to 1300, 1400 and 1500 °C, respectively, and sintering was completed at these top temperatures with 2 h dwell time. The cooling down to room temperature was accomplished in 5 h.

The functionalization of the YSZ membranes was carried out according to a procedure described elsewhere [12,13]. The functionalization was performed using a hydroxylation step with a Piranha solution (a mixture of concentrated sulfuric acid, H_2SO_4 99.99%, with hydrogen peroxide, H_2O_2 99.99%, in a volume ratio of 3:1). Then the membranes were immersed in a 0.2 M water solution of 3-aminopropyl triethoxysilane, (APTES, ABCR Gute Chemie) and incubated for 24 h. After functionalization, the membranes were washed until the rinsing water reached pH of 7.0 and then dried for 24 h at 70 °C.

2.5. Microstructure and surface characterization

The membrane microstructure was observed in a scanning electron microscope (SEM Camscan, series 2, Obducat CamScan) at 20 kV after sputtering the samples with gold. After functionalization, microstructural observations were carried out in a scanning electron microscopy (SEM) with electron dispersion X-ray (EDX) for chemical analysis (Zeiss Supra 40 SEM, Carl Zeiss) with an acceleration voltage of 0.5 kV. The images were treated (ImageJ software) to estimate the surface pore size on the structure by using 20 measures for each membrane composition Fig. s2 [14]. The pore size distribution (micro-meso-macro pore ranges from 0.01 to 100 μm) and open porosity were determined using mercury intrusion porosimetry (Pascal 140/440, Porotec). The specific surface area (SSA) was determined by nitrogen adsorption and desorption and calculated from the isotherms measured at 77 K (Belsorp-Mini, Bel).
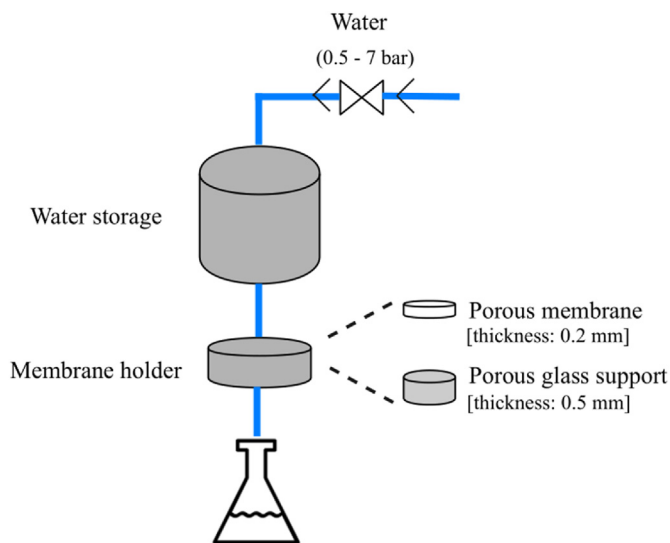
Fig. 1. Schematic diagram of the device used in the determination of water permeance.

Hydrophilicity and hydrophobicity characteristics were studied by water and n-heptane vapor adsorption and described in detail elsewhere [15]. The assays were carried out by exposing ~0.5 g of the sample, after crushing in a mortar, to deionized water and heptane (C_7H_{16}, Sigma Aldrich) vapor in a closed vessel for 24 h at 22 °C. Vapor adsorption, expressed in mmol·g^{-1} was determined by changing the sample weight.

2.6. Water flux and permeance

Membrane permeance was determined using a dead-end microfiltration module, displayed in Fig. 1. The water was pumped through the membrane holder and the pressures were adjusted by using manually operated valves. The permeate flux was measured with a volumetric flask, as described elsewhere [16].

The permeate flux rate was calculated using Eq. (1).

$$J = \frac{dV}{dt}\frac{1}{A_m} \tag{1}$$

where J is the transient permeate flux (Lh^{-1}m^{-2}), dV is the differential volume (L), dt is the differential time (h), and A_m is the effective membrane surface area (m^2).

The permeance (Q, L·h·m^{-2}Pa) – a flux normalized for a given driving force – can be calculated by Eq. (2):

$$Q_i = \frac{J}{\Delta p} \tag{2}$$

where Δp is the pressure gradient along the flow direction (bar).

3. Results and discussion

3.1. Rheology and stability of suspensions

Fig. 2 shows the shear stress in dependency of shear rate curves of the YSZ_PF and YSZ_NPF slurries, i.e., with pore former and without pore former, respectively. The rheological behavior in both cases is pseudoplastic, which is desirable for tape casting processes [1]. Slurries with this behavior have a viscosity value decreasing with the shear rate when the suspension flows through the blade. After flow under the blade, the shear rate returns to zero and the viscosity increases [1,17], which helps to maintain the thickness and shape of the slurry after casting.

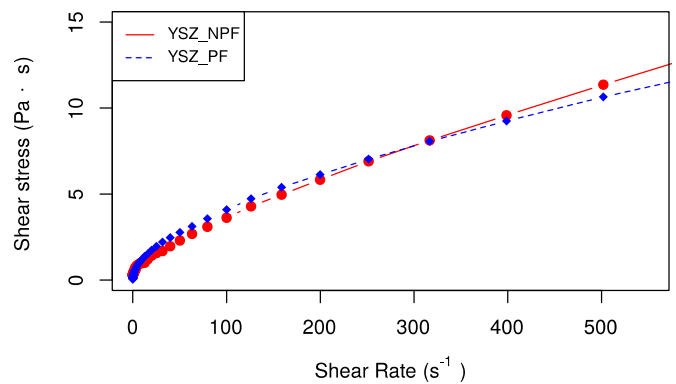The zeta potential *vs.* pH of the YSZ aqueous suspension with

Fig. 2. Shear stress in dependency of shear rate of the slips with (YSZ_PF) and without pore former (YSZ_NPF).
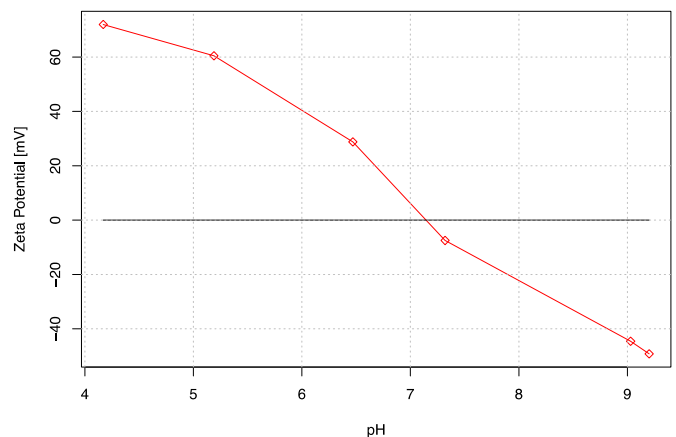

Fig. 3. Zeta potential in dependency of pH of YSZ powder in water with 1 wt% dispersant.

dispersant is shown in Fig. 3. Basically, the higher the zeta potential, the stronger the particle repulsive forces, which result in a more stable slurry, particularly when values over 30 mV are reached [18]. This promotes the manufacturing of homogeneous ceramic tapes with higher homogeneity and fewer defects [17]. The slurry presented a zeta potential in a range between 60 and -50 mV. The isoelectric point (IEP) was found at a pH of 7.25. Usually, the addition of dispersant reduces the IEP and makes the slurry stable at lower pH values. The pH of the slurry after homogenization of all components was already in the zeta potential range for stable suspensions (pH = 9, Fig. 3). Thus, no pH correction was necessary.

3.2. Microstructural analysis

Fig. 4 shows the SEM cross-section and top surface of the sintered tapes (YSZ_PF and YSZ_NPF) at 1300, 1400 and 1500 °C. The SEM images of the membranes sintered at 1400 °C (Fig. 4c) presented a larger pore size with values around 1.40 µm. This behavior is related to the sintering step when a higher interconnection between pores results in bigger cavities or channels during grain growth [19].

The pore coalescence during sintering might contribute to the enlargement of the pores in the matrix. Zirconia usually densifies above 1170 °C, depending on the original particle size, and the shape or size of green bodies [20]. For zirconia nanoceramics, sintering temperatures ranging from 1000 °C [21] up to 1600 °C [22] have been reported. Moreover, the tapes sintered at 1500 °C (Fig. 4d) show a smaller average pore size of 0.81 µm, due to the structure accommodation during phase transition. The membranes also showed a thickness ranging from 0.24 mm up to 0.37 mm after sintering, without delamination
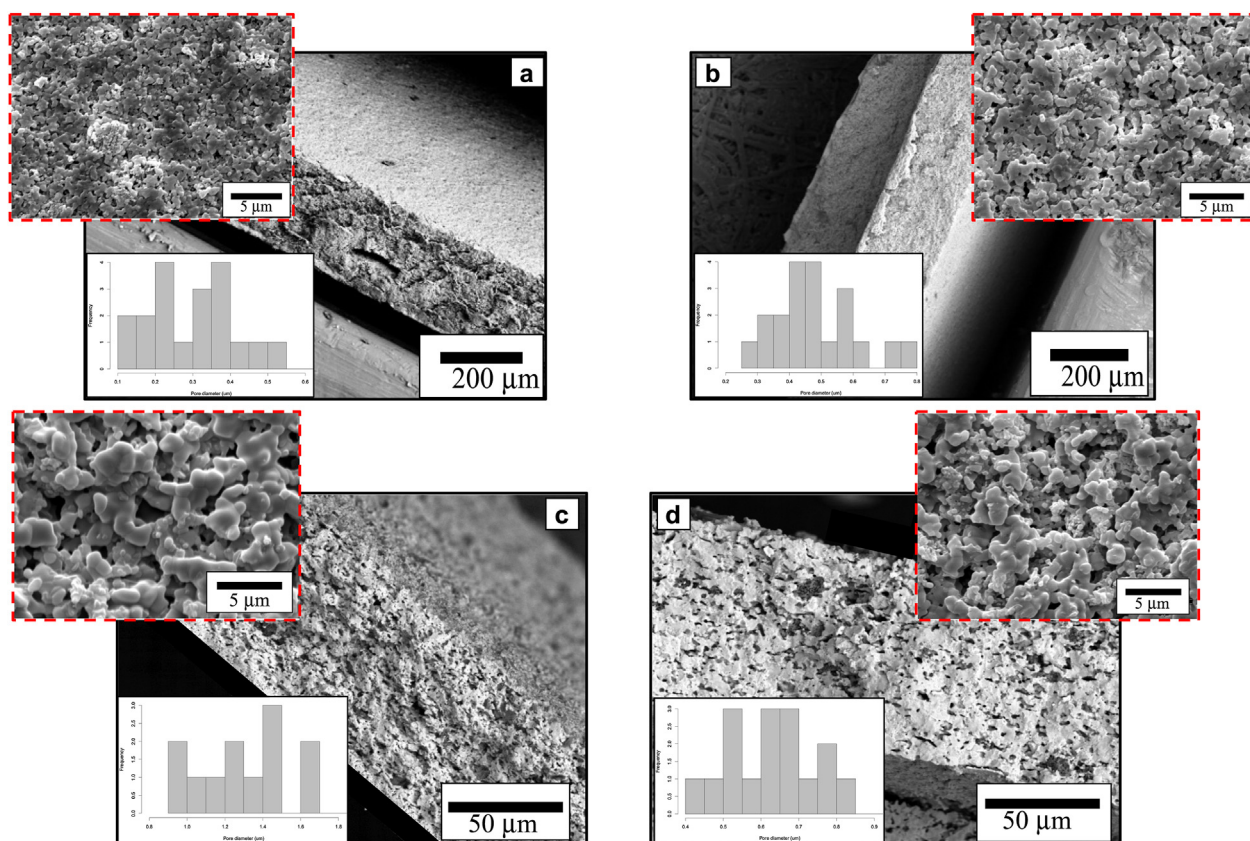
Fig. 4. SEM images from the cross section and the top surface (inserts) of the tapes without pore former (a) and 6 wt % pore former (PMMA) (b)–(d) the tapes sintered at 1300, 1400 and 1500 °C.

of the two layers.

The addition of PMMA hindered high densification. The PMMA particles have an average size of 3.4 μm and were eliminated before sintering started. The pores may coalesce during sintering so that the pore size increased with PMMA. The greater the pore size, the lower the driving force for sintering and shrinkage [22]. A microstructure with homogeneously distributed small pores was found. A narrow distribution with an average pore size of 0.18 μm was observed (Fig. 4a). However, an increase of pore size up to 0.62 μm was noticed (Fig. 4b), which might be related to the addition of pore former, leaving voids after debinding. The irregularly shaped pores correspond roughly to the shape of the PMMA particles (3.4 μm) used as sacrificial pore formers, as observed elsewhere [23] with a range of pores from 0.15 up to 1.2 μm. A synergistic effect between temperature and sacrificial pore former was noticed. At increasing temperatures, zirconia tends to densify, which enhances the mechanical strength but closes the pores. However, the sacrificial pore former acts as a place holder preventing full densification during grain growth [5,19].

3.3. Porosity and pore size distribution

Fig. 5 shows the results obtained by mercury intrusion porosimetry for the sintered tapes, with a pore range between 0.01 and 100 μm. The lower values (0.01 μm) correspond to the binders that were burned out before sintering [22]. On the other hand, higher values in a range of 100 μm are probably related to cracks and defects present in the membranes. YSZ_PF_1400 and YSZ_PF_1500 samples presented a bimodal pore size distribution with an average pore size of 1.4 and 0.8 μm, respectively, indicating the collapse of the pores. Comparable values were extracted by image analysis. For the samples YSZ_NPF_1300 and YSZ_PF_1300, sintered at the lowest temperature, bimodal distributions were obtained with average values of 0.2 and
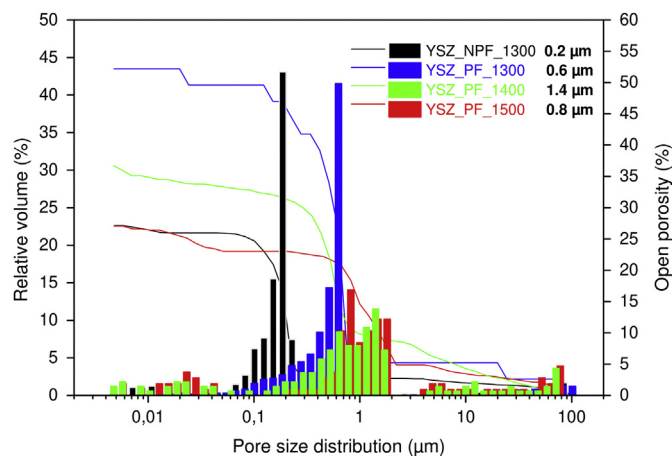

Fig. 5. Pore size distribution and open porosity of the membrane samples sintered at different temperatures.

0.6 μm, respectively. Excluding the low fractions of large pores, all the samples showed pores ranging between 0.1 and 1.5 μm, suggesting a homogeneous pore distribution throughout the membrane.

The open porosity varies in a range between 27% and 51% depending on the use of PMMA and the sintering temperature. The PMMA content had a positive effect on the open porosity, as also observed by Santa Cruz et al. [24]. Nevertheless, within the range of sintering temperatures used in this work, open pores with diameters between 0.2 to 1.4 μm could be reached, which is a positive effect regarding the desired application. The pore size can be controlled at first by altering the sacrificial pore former and secondly by the sintering temperature.

Table 2
Specific surface area and isotherms types.

Sample	SSA ($m^2 \cdot g^{-1}$)	Isotherm type
YSZ_NPF_1300	1.2	II
YSZ_PF_1300	1.7	II
YSZ_PF_1400	0.8	II
YSZ_PF_1500	0.2	II

3.4. BET surface analysis

Nitrogen adsorption isotherms and specific surface area (SSA) of the sintered membranes were investigated to determine the influence of the sintering time on microstructure, as shown in Table 2. Fig. S1 presents the specific surface area and isotherm type obtained from the nitrogen adsorption isotherms for the different samples. The membrane sintered at 1300 °C without PMMA achieved a specific surface area of 1.2 $m^2 \cdot g^{-1}$ (YSZ_NPF_1300). This SSA is increased to around 1.7 $m^2 \cdot g^{-1}$ (YSZ_PF_1300) with the addition of 6 wt.% pore former. On the other hand, for the sample sintered at 1400 °C, SSA showed a considerable reduction to 0.8 $m^2 \cdot g^{-1}$ (YSZ_PF_1400). A further increase in sintering temperature, at 1500 °C, caused a decrease in SSA to 0.2 $m^2 \cdot g^{-1}$ (YSZ_PF_1500). Comparable SSA values were reported in the literature for monoclinic zirconia as expected for ZrO_2 materials [25]. All the isotherms can be classified as type II which is typical for macroporous solids showing macropores filling, but no multilayer adsorption [26].

3.5. Characterization of the membranes after functionalization

Membrane surfaces after functionalization are shown in Fig. 6, with EDX results for each composition. As expected, the YSZ_PF_1300 sample (Fig. 6a) did not present any silicon or nitrogen atoms, which are associated with aminosilane (APTES) precursor. In all functionalized membranes (Fig. 6b, c and d) Si and N were detected, evidencing the success in APTES deposition on the surface, as also shown in the literature [26]. When compared to the non-functionalized membranes (Fig. 4), the functionalized surfaces seem smoother, although some small aggregates can also be observed, which may correspond to an excess of APTES deposited on the membrane surface.

3.6. Hydrophobicity and hydrophilicity

The vapor adsorption of polar (water) and non-polar (n-heptane) solvents was carried out to determine the surface properties of the membranes as displayed in Fig. 7. All the samples presented a hydrophilic behavior, as expected for oxide ceramics [27]. YSZ_NPF_1300 membranes tend to be more hydrophilic with sorption values of 0.49 $mmol \cdot g^{-1}$ and 0.18 $mmol \cdot g^{-1}$ of water and n-heptane, respectively. Water adsorption was 2.7 higher than n-heptane uptake. Ratio values higher than 1 indicate hydrophilic surface characteristics. Regarding YSZ_PF_1300 membranes, sintered at the same temperature, but with added pore former, a hydrophilic surface was also obtained. The molar ratio of water to heptane uptake (w/h) was equal to 2.5, indicating that neither the porosity nor the pore size plays a role in the surface properties. The average amount of water and n-heptane adsorbed by YSZ_PF_1400 was 1.47 $mmol \cdot g^{-1}$ and 0.30 $mmol \cdot g^{-1}$, respectively, resulting in a w/h ratio of 4.8 times. Nevertheless, for the YSZ_PF_1500 membranes, values of 2.53 and 0.52 $mmol \cdot g^{-1}$ were obtained for water and n-heptane, representing an increment of 4.4 times in hydrophilicity.

The assays of vapor adsorption of polar (water) and non-polar (n-heptane) solvents on membrane samples were also carried out to determine the surface properties after silanization (Fig. 7). All functionalized samples showed a higher hydrophilic behavior than the non-functionalized membranes, which is expected after APTES deposition [28,29]. APTES_YSZ_13 membranes presented a water uptake 12.5 higher than that of n-heptane. The membranes sintered at 1400 °C (APTES_YSZ_14) presented a ratio of water to heptane uptake equal to 7.6 and in the samples sintered at 1500 °C (APTES_YSZ_15), a ratio of 5.9 was achieved. These values correlate with the functionalized groups present on the surface, as confirmed by EDX measurements (Fig. 6), and agree with the increment in water permeability results discussed in item 3.7. In Fig. 6, partial filling of bigger pores with APTES can be noticed. Beside the surface groups, the building of a cross-linked APTES network and with that a slight increase of SSA of the membranes of the functionalized membrane (not measured) could not be excluded as one reason for the higher hydrophilicity (Fig. 7).

3.7. Water permeation

The membrane performance was evaluated in a dead-end permeation device to measure the water permeate flux before and after functionalization. All membranes showed good mechanical stability and are suitable for application at pressures lower than 1 bar. Fig. 8 and 9 display the results respectively before and after functionalization, at three different transmembrane working pressures (0.5, 0.75 and 1 bar). For the non-functionalized YSZ_NPF_1300 sample, a low transient permeate flux at the three different pressures can be noticed. This result agrees with the porosity (27%) and the average pore size of the sample 0.2 μm. In contrast, the YSZ_PF_1300 sample showed a slight increase in the transient permeate flux, due to higher porosity (51%) and pore size (0.6 μm) when compared with the previous case. The same trend is observed for YSZ_PF_1400. The transient permeate flux of YSZ_PF_1500, which has an average pore size of 0.8 μm and porosity of 27% was similar to the two first samples (YSZ_NPF_1300 and YSZ_PF_1300). Even though the porosity plays an important role in the water permeability, the average pore size seems to have a stronger influence on the permeate flux. The increasing water flux as a function of pore size and porosity is also reported by previous studies, for instance in the dead-end microfiltration of yeast using alumina membranes [16]. Comparable water permeances (260 $Lm^{-2}h^{-1}$) were also previously reported for alumina membranes with a pore size of 0.2 μm, which is in the same range as the present study [30].

After functionalization, the performance of the membranes was evaluated for comparison with the control membranes. The same parameters were considered, and the transient flux was calculated. Fig. 9 displays the functionalized membranes performance at three different working pressures (0.5, 0.75 and 1 bar).

YSZ_NPF_sample was not evaluated due to the average pore size, which was very small (0.2 μm) and would even decrease after functionalization, making the sample unfit for microfiltration processes. Although the pore size of the functionalized membranes has not been analyzed in detail, the decrease of pore size after surface functionalization was observed and discussed by McCool and Desisto [31] for silica membranes. The functionalized samples sintered at 1300 (APTES_YSZ_13) and 1500 °C (APTES_YSZ_15) with added pore former showed higher fluxes compared to the same samples before functionalization. On the other hand, APTES_YSZ_14 showed the highest water permeate flux in comparison with the non-functionalized membranes. This behavior can be explained by the high average pore size as well as the higher porosity of APTES_YSZ_14 membrane compared to the two other membranes APTES_YSZ_13 and APTES_YSZ_15. When the surface is modified with APTES, amino groups (NH_2) are attached to the membrane surface, these groups increase the interaction with water and facilitate water permeation through the pores, as confirmed by water up-take in Fig. 7.

Extruded ZrO_2 capillaries with a pore size of 145 nm, an open porosity of 50% and SSA of 5.4 $m^2 g^{-1}$ before and after functionalization showed an increment from 150 $Lm^{-2}h^{-1}bar^{-1}$ after APTES functionalization [15], what proves the fact that the surface functionalization of
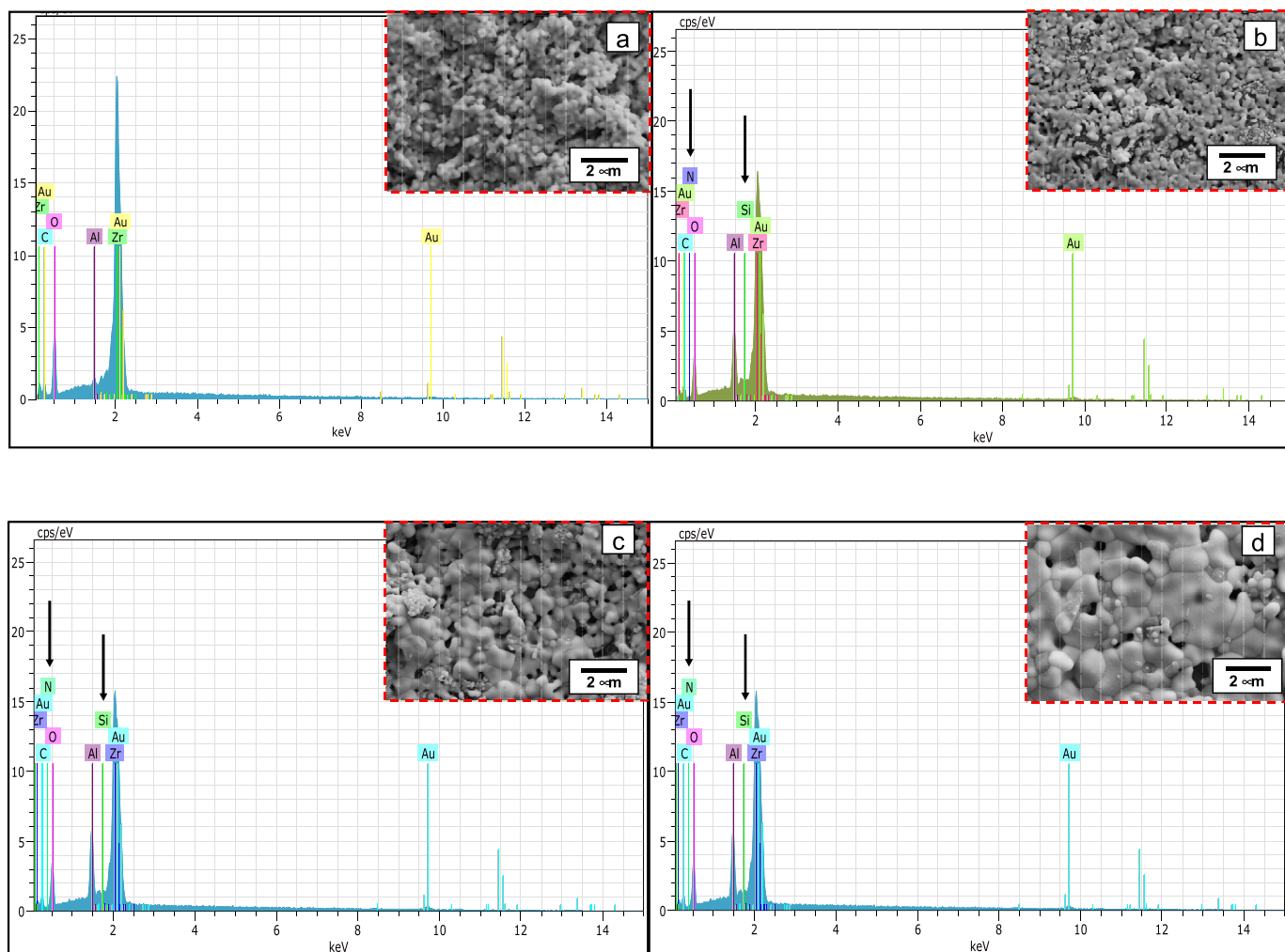
Fig. 6. SEM images and EDX (inserts) of the tapes without pore former (a) and 6 wt % pore former (PMMA) (b)–(d) the tapes sintered at 1300, 1400 and 1500 °C after functionalization.
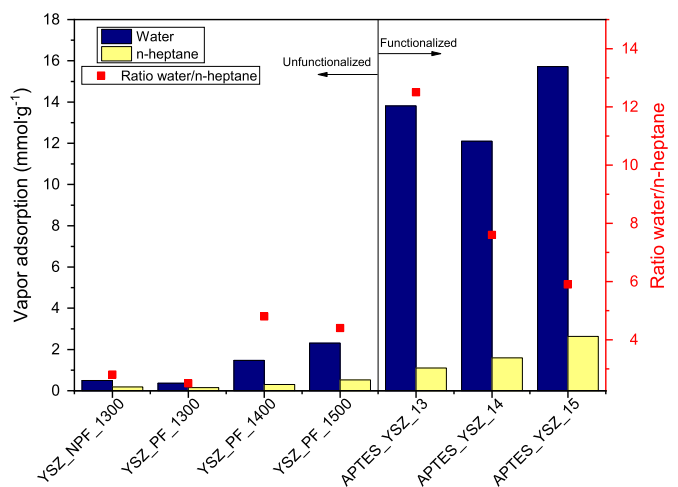

Fig. 7. Water and n-heptane vapor adsorption at 22 °C and molar ratio of maximum water/n-heptane adsorption before (left of the vertical line) and after (right of the vertical line) functionalization.
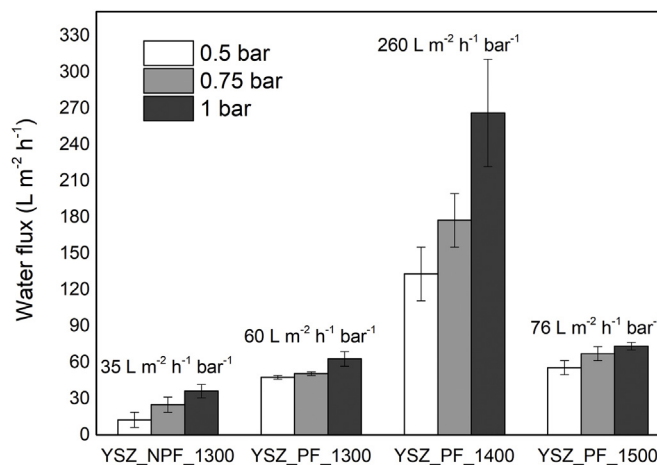

Fig. 8. Permeate flux performance of non-functionalized membranes at three different working pressures (0.5, 0.75 and 1.0 bar). Values above each set of bars stand for the water permeance calculated by the slope of permeate flux vs. transmembrane pressure line.

the membranes plays a significant role in the water flux essays, while all other properties remain unchanged. To the best of our knowledge, the increase of water permeance in ZrO_2 membranes manufactured by aqueous tape casting after membrane functionalization with APTES has
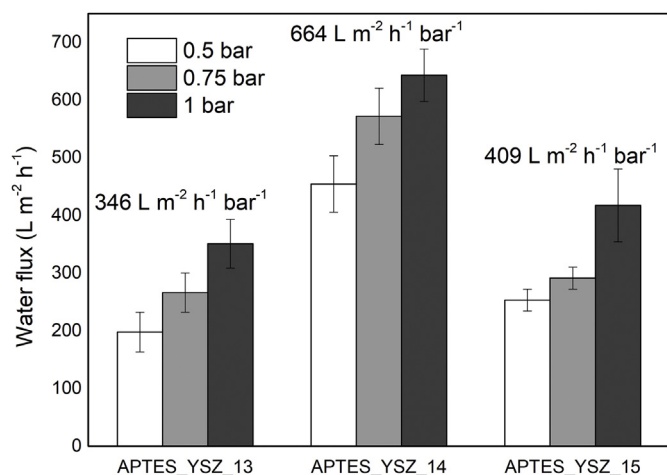
not been described elsewhere.

Fig. 9. Permeate flux performance of functionalized membranes at three different working pressures (0.5, 0.75 and 1.0 bar). Values above each set of bars stand for the water permeance calculated by the slope of permeate flux vs. transmembrane pressure line.

4. Conclusions

In this work, yttria-stabilized zirconia porous membranes were successfully produced by aqueous tape casting. PMMA and other additives did not affect the dispersion properties of the YSZ powder, which were governed by the adsorbed dispersant providing an electrosteric stabilization.

The pH at the isoelectric point was 7.25 for the zirconia aqueous suspension. The slurry at pH = 9 yielded a zeta potential of −45 mV, confirming that it was colloidally stable. The rheological behavior of the slurry was pseudoplastic, which is desirable for tape casting.

The open porosity was controlled by using PMMA as a sacrificial pore former and by the sintering temperature. Membranes with open porosity from 27% to 51%, pore sizes in the range of 0.2 to 1.5 μm and specific surface area of 1–2 $m^2 \cdot g^{-1}$ were obtained. Different values of open porosity and average pore size played a role in water fluxes, that reached up to 260 $Lm^{-2}h^{-1}$ at 1.0 bar for unfunctionalized membranes and 642 $Lm^{-2}h^{-1}$ at 1.0 bar for the functionalized ones.

Water and n-heptane vapor adsorption showed that the membranes present a hydrophilic character, similar to that of oxide ceramic membranes. Functionalization was performed successfully and confirmed by SEM-EDX elemental analysis. The functionalized membranes exhibited an increase of water flux up to 5-fold.

The average pore size and porosity play a significant role in water permeability, for both functionalized and non-functionalized samples. However, the average pore size seems to have a stronger influence on permeability than the porosity. The range of pores of the tailored surface and the functionalization procedure indicated a potential application of these membranes for microfiltration processes.

Declaration of competing interest

The authors declare that they have no known competing financial interests or relationships that could have appeared to influence the work reported in this paper.

Acknowledgments

Appendix A. Supplementary data

Supplementary data to this article can be found online at https://doi.org/10.1016/j.ceramint.2020.03.162.

References

[1] R.E. Mistler, E.R. Twiname, Tape Casting: Theory and Practice, (2000).
[2] R.K. Nishihora, P.L. Rachadel, M.G.N. Quadri, D. Hotza, Manufacturing porous ceramic materials by tape casting—a review, J. Eur. Ceram. Soc. 38 (2018) 988–1001, https://doi.org/10.1016/j.jeurceramsoc.2017.11.047.
[3] D. Hotza, P. Greil, Aqueous tape casting of ceramic powders, Mater. Sci. Eng. a-Structural Mater. Prop. Microstruct. Process. 202 (1995) 206–217, https://doi.org/10.1016/0921-5093(95)09785-6.
[4] F. Bouzerara, A. Harabi, B. Ghouil, N. Medjemem, B. Boudaira, S. Condom, Elaboration and properties of zirconia microfiltration membranes, Procedia Eng 33 (2012) 278–284, https://doi.org/10.1016/j.proeng.2012.01.1205.
[5] A.R. Studart, U.T. Gonzenbach, E. Tervoort, L.J. Gauckler, Processing routes to macroporous ceramics: a review, J. Am. Ceram. Soc. 89 (2006) 1771–1789, https://doi.org/10.1111/j.1551-2916.2006.01044.x.
[6] S. Kroll, L. Treccani, K. Rezwan, G. Grathwohl, Development and characterisation of functionalised ceramic microtubes for bacteria filtration, J. Membr. Sci. 365 (2010) 447–455, https://doi.org/10.1016/j.memsci.2010.09.045.
[7] L. Treccani, T. Yvonne Klein, F. Meder, K. Pardun, K. Rezwan, Functionalized ceramics for biomedical, biotechnological and environmental applications, Acta Biomater. 9 (2013) 7115–7150, https://doi.org/10.1016/j.actbio.2013.03.036.
[8] P. Arora, R. Jain, K. Mathur, A. Sharma, A. Gupta, Synthesis of Polymethyl Methacrylate (PMMA) by Batch Emulsion Polymerization, vol. 4, (2010), pp. 152–157.
[9] V. Moreno, J.L. Aguilar, D. Hotza, 8YSZ Tapes produced by aqueous tape casting, Mater. Sci. Forum 727–728 (2012) 752–757 https://doi.org/10.4028/www.scientific.net/MSF.727-728.752.
[10] M. Cologna, V.M. Sglavo, M. Bertoldi, Sintering and deformation of solid oxide fuel cells produced by sequential tape casting, Int. J. Appl. Ceram. Technol. 7 (2010) 803–813, https://doi.org/10.1111/j.1744-7402.2009.02390.x.
[11] J. Aguilar-Arias, D. Hotza, P. Lenormand, F. Ansart, Planar solid oxide fuel cells using PSZ, processed by sequential aqueous tape casting and constrained sintering, J. Am. Ceram. Soc. 96 (2013) 3075–3083, https://doi.org/10.1111/jace.12559.
[12] J. Bartels, M.N. Souza, A. Schaper, P. Árki, S. Kroll, K. Rezwan, Amino-functionalized ceramic capillary membranes for controlled virus retention, Environ. Sci. Technol. 50 (2016), https://doi.org/10.1021/acs.est.5b05124 1973–1981.
[13] S. Kroll, C. Brandes, J. Wehling, L. Treccani, G. Grathwohl, K. Rezwan, Highly efficient enzyme-functionalized porous zirconia microtubes for bacteria filtration, Environ. Sci. Technol. 46 (2012) 8739–8747, https://doi.org/10.1021/es3006496.
[14] C.A. Schneider, W.S. Rasband, K.W. Eliceiri, NIH Image to ImageJ: 25 years of image analysis, Nat. Methods 9 (2012) 671, https://doi.org/10.1038/nmeth.2089.
[15] T. Prenzel, T.L.M. Guedes, F. Schlüter, M. Wilhelm, K. Rezwan, Tailoring surfaces of hybrid ceramics for gas adsorption - from alkanes to CO2, Separ. Purif. Technol. 129 (2014) 80–89, https://doi.org/10.1016/j.seppur.2014.03.029.
[16] S. Mahesh Kumar, S. Roy, Filtration characteristics in dead-end microfiltration of living Saccharomyces cerevisiae cells by alumina membranes, Desalination 229 (2008) 348–361, https://doi.org/10.1016/j.desal.2007.11.011.
[17] Colloid science, in: R.J. HUNTER (Ed.), Zeta Potential Colloid Sci. Academic Press, 1981, , https://doi.org/10.1016/B978-0-12-361961-7.50001-8.
[18] L.B. Robert, J. Pugh, Surface and Colloid Chemistry in Advanced Ceramics Processing, n.d.
[19] B.R.M. German, Sintering Science : an Historical Perspective, (n.d.).
[20] Andrew Fletcher, Zirconia, (1993).
[21] D. Hotza, D.E. García, R.H.R. Castro, Obtaining highly dense YSZ nanoceramics by pressureless, unassisted sintering, Int. Mater. Rev. 60 (2015) 353–375, https://doi.org/10.1179/1743280415y.0000000005.
[22] M.P. Albano, L.B. Garrido, K. Plucknett, L.A. Genova, Processing of porous yttria-stabilized zirconia tapes: influence of starch content and sintering temperature, Ceram. Int. 35 (2009) 1783–1791, https://doi.org/10.1016/j.ceramint.2008.10.003.
[23] M.P. Albano, L.A. Genova, L.B. Garrido, K. Plucknett, Processing of porous yttria-stabilized zirconia by tape-casting, Ceram. Int. 34 (2008), https://doi.org/10.1016/j.ceramint.2007.07.028 1983–1988.
[24] H. Santa Cruz, J. Spino, G. Grathwohl, Nanocrystalline ZrO2ceramics with idealized macropores, J. Eur. Ceram. Soc. 28 (2008) 1783–1791, https://doi.org/10.1016/j.jeurceramsoc.2007.12.028.
[25] G. Witz, V. Shklover, W. Steurer, S. Bachegowda, H.-P. Bossmann, Phase evolution in yttria-stabilized zirconia thermal barrier coatings studied by rietveld refinement of X-ray powder diffraction patterns, J. Am. Ceram. Soc. 90 (2007) 2935–2940, https://doi.org/10.1111/j.1551-2916.2007.01785.x.
[26] J. Keller, R. Staudt, Gas adsorption equilibria - experimental methods and adsorption isotherms, https://doi.org/10.1007/b102056, (2005).
[27] A.V. Rudakova, M.V. Maevskaya, A.V. Emeline, D.W. Bahnemann, Light-controlled

ZrO 2 surface hydrophilicity, Sci. Rep. 6 (2016) 2–6, https://doi.org/10.1038/srep34285.

[28] J.A. Howarter, J.P. Youngblood, Optimization of silica silanization by 3-aminopropyltriethoxysilane, Langmuir 22 (2006) 11142–11147, https://doi.org/10.1021/la061240g.

[29] F. Wang, H. Zhu, H. Zhang, H. Tang, J. Chen, Y. Guo, Engineering Effect of surface hydrophilic modification on the wettability , surface charge property and separation performance of PTFE membrane, J. Water Process Eng. 8 (2015) 11–18,

https://doi.org/10.1016/j.jwpe.2015.08.004.

[30] S. Rezaei, H. Abadi, M. Reza, M. Hemati, F. Rekabdar, T. Mohammadi, Ceramic membrane performance in micro filtration of oily wastewater, Desalination 265 (2011) 222–228, https://doi.org/10.1016/j.desal.2010.07.055.

[31] B.B.A. Mccool, W.J. Desisto, Amino-functionalized silica membranes for enhanced carbon dioxide permeation **, https://doi.org/10.1002/adfm.200400293, (2005) 1635-1640.